AAS 23-155

GIMBAL BEARING FRICTION IN THE SLS CORE STAGE THRUST VECTOR CONTROL SYSTEM

Colter W. Russell[*], Jeb S. Orr[†], Jeff Brouwer[‡], Stephen G. Ryan[§], and Nathaniel Stepp[¶]

The Space Launch System (SLS) Core Stage Thrust Vector Control (TVC) system is comprised of eight mechanical feedback Shuttle heritage Type III TVC actuators that vector the four Shuttle heritage RS-25 engines about a Shuttle heritage gimbal block/bearing. The MSFC Controls community has long regarded gimbal friction to be a negligible effect on the overall control of gimbaled RS-25 engines. This is corroborated by Space Shuttle test and flight data that does not appear to show degraded effects, nor limit cycling at the end of the shuttle flight. For this reason, friction was not expected to be a driving factor of performance and control of the reused RS-25 engines aboard the SLS. However, after test data showed a large shift in frequency behavior and a highly damped step-response in the time series, there was further investigation into what could have caused this behavior. Heritage friction models used in previous gimbal and ball bearings were evaluated such as Coulomb, Dahl and LuGre, but the single degree of freedom friction models alone were not enough to explain the behavior and shifts seen in the test data.

This paper presents the additional findings and modeling efforts regarding friction on the RS-25 engines. Using the Two Actuator Operational Simulation (TAOS), the difference from modeling separate friction degrees of freedom to coupled degrees of freedom was investigated to deduce the effects of one axis's movement on the other. Next, due to the vibration environment, a modified LuGre model has been proposed that adds an additional term to decrease the friction coefficient at low engine velocity amplitudes. Lastly, the addition of the stiffness in each half of the gimbal bearing has increased modeling fidelity by also adding the effect on the gimbal bearing bending in compliance to both the friction torque on the surface of the gimbal bearing and the actuator force that is forcing the engine in a specified direction. Through these effects, the time and frequency domain behavior seen in test can be characterized accurately.

1 INTRODUCTION

The RS-25 gimbal bearing has a long heritage of use on the Space Shuttle program. Throughout its flight history, the bearing was generally observed to operate as a simple pivot devoid of any friction effects. While pre-flight testing confirmed the presence of gimbal friction, the available documentation indicates that the levels were acceptable to the flight control engineers. Specifically, there were no degraded transient responses, nor was there limit cycling observed near the end of flight. With all the STS post-flight data corroborating these findings, modeling of gimbal friction

[*]Flight Systems Technical Staff, Mclaurin Aerospace (Jacobs ESSCA), Knoxville, TN
[†]Space Launch System Flight Dynamics and Control Technical Specialist (Mclaurin Aerospace / ESSCA), Knoxville, TN
[‡]Navigation, Guidance, and Control Subject Matter Expert, Troy 7, Inc. (Jacobs ESSCA), Huntsville, AL
[§]SLS Chief Engineer's Office (MTS CPSS), Huntsville, AL
[¶]TVC Controls Engineer, NASA MSFC, Huntsville, AL

received little attention for the RS-25 engine during its application on the Space Shuttle vehicle [20, 21, 22, 23].

The Space Launch System (SLS) used the Green Run Hot Fire (GRHF) test to evaluate the core stage design and validate the performance of many of its constituent systems. The test profile included ambient (non-thrusting) test and hot fire (thrusting) TVC check cases. The first test case supported the hypothesis that friction would be a negligible factor, as there was no thrust load on the gimbal bearing to engage friction between the bearing surfaces. On the other hand, the thrusting (hot fire) test case was evaluated to verify that friction would not play a significant role in the SLS TVC performance. To the surprise of the flight control engineering team, friction was clearly present and much more impactful to the TVC system performance than previously suspected. This test anomaly led to the formation of a special analysis team whose charter was, in part, to develop a model of friction that most closely reproduced the response shown in test, so as to accurately predict the flight performance. The candidate models, including Coulomb, Dahl, and LuGre, have heritage use in aerospace applications [1, 2, 3, 4, 5, 6]. However, these models alone could not accurately describe the observed frequency and transient response characteristics seen during Green Run Hot Fire.

Of particular interest following GRHF was the synthesis of a physics-based model that replicated the GRHF time and frequency domain characteristics. The first phenomenon of interest was the effect of coupled degrees of freedom (DoF) of the gimbal, e.g., friction in three dimensions tangent to the gimbal bearing contact surface instead of separating it into individual axes. Other effects such as an offset center of mass a non-diagonal inertia tensor can amplify the coupling between adjacent TVC degrees of freedom. Thereafter, the local compliance of the gimbal structure was a key factor in reproducing the response seen in the test data; that is, the dynamics of the gimbal structure itself must be accounted for under high thrust loading conditions Finally, the effects of the vibration environment including that due to thrust oscillation, structural resonances, and reflected acoustics appears to have a significant impact on the friction characteristics. Through a modification to the LuGre model to include the effects of vibration, a model was developed that faithfully reproduces the observed response at GRHF.

2 GREEN RUN HOT FIRE TVC OBSERVATIONS

The Green Run test series was employed to evaluate all the necessary stage subsystems of the SLS Core Stage before stacking the vehicle for flight. Two tests in the Green Run series evaluated the TVC system performance. These were the ambient vectoring test of the engines (“TC7”) and the Green Run Hot Fire (GRHF) test. Both tests employed a command sequence that included a set of discrete sines followed by step commands. The flight controls team expected differences in engine and actuator position (piston) response between the two test conditions; however, it was expected based on pre-test models that both sets of data would be in family with one another and with prior laboratory test data. Test data was found to be significantly out of family, and the TVC time and frequency-domain performance requirements were not met in both test conditions.

Compared with pre-test predictions, the actuator response in TC7 (ambient) conditions behaved like the expected damped second order system, except with a consistently larger degree of overshoot. Frequency response followed an expected response curve shown in the Figure 1. The notch

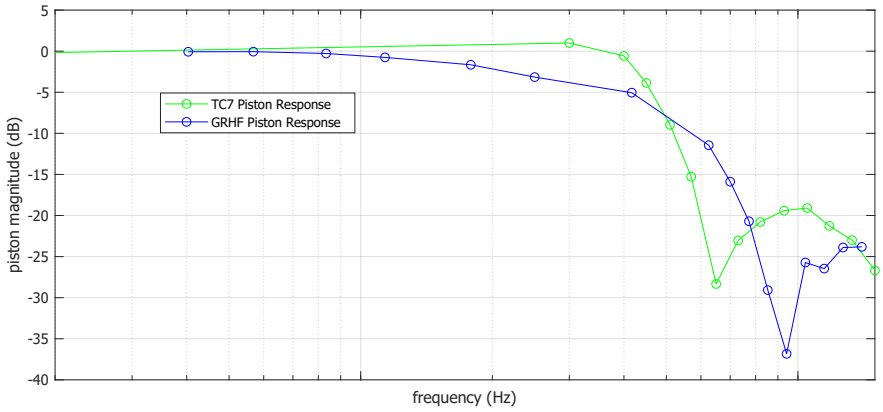

Figure 1. Ambient and GRHF gain responses

characteristic that is seen at the lower frequency is a measure of the load resonance determined by the engine inertia J_n, linear load stiffness K_L, moment arm R and engine angular stiffness K_n. The expression for the load resonance frequency is given in Equation 1 [19]. The load stiffness K_L, which contributes most significantly to the load resonance, is a series approximation of the stiffnesses that are in the actuator load path, such as the engine attach stiffness, backup structure stiffness, and actuator stiffness (excluding oil compressibility). This stiffness can be modeled in parallel with the engine angular stiffness resulting from gravitational torques and the hydrostatic pressure of the engine propellant feedlines.

$$\omega_L = \sqrt{\frac{K_L R^2 + K_n}{J_n}} \tag{1}$$

Pre-test predictions of the load stiffness supported a notch frequency (load resonance) closer to 9 Hz, based primarily on data from the core stage finite element model (FEM). The most significant finding of the ambient vectoring test was that the apparent load resonance frequency was around 6.5 Hz, which could only be produced by a structural stiffness about half the value of the pre-test predictions. Time domain results are covered in reference [16] by Wall et. als

After the load stiffness and parameters had been adjusted to match the TC7 data, the team ran the GRHF test and expected to find similar performance. Surprisingly, almost all aspects of the response had changed drastically in the presence of thrust loading. The load resonance notch shifted to 9.5 Hz as seen in Figure 1. The frequency response also exhibited degraded gain and phase performance in the lower frequency band. As discussed in the companion paper[16], the step response now appeared to be heavily damped and showed amplitude dependence between the 0.2, 0.4 and 0.6 degree step commands. This difference in average engine position across all engines is shown in Figure 2. Note that these are normalized by command amplitude in order to compare the amplitude dependence between each of the commands. To properly bound the TVC performance and support rationale for flight readiness, a conservative approach to the effects of friction was needed. This started the SLS flight controls and TVC teams on a path to determine the underlying causes for the difference in behaviors and develop models that could sufficiently represent the load-dependent friction and stiffness effects seen in the tests.

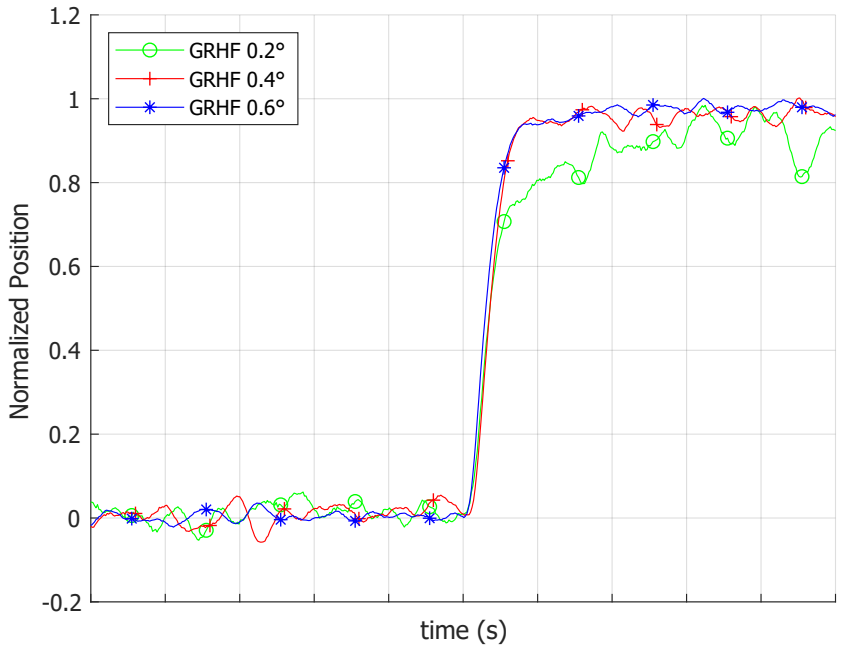

Figure 2. Average engine position for each of the positive engine steps

3 HISTORICAL BACKGROUND

Friction is hard to characterize and account for even with current advances in contact mechanics, tribology, material science, and the many other fields that intersect to describe it. As friction is a function of many phenomena, approximations to its behavior in specific regimes have become commonplace. Many models have been created [1, 2], both dynamic and static, to describe the effect of friction as two surfaces move relative to each other. Some are static models that oppose motion in the same way no matter the position or velocity state, while others are state-dependent and have different behavior in different regimes of operation of the system. In complex systems, such as rocket engine gimbal bearings, it is important to model the physical phenomena affecting the system, but not over fit the model to the available data. To ensure a sufficiently proper characterization, the authors approached the SLS gimbal friction problem by starting with the simplest model and adding fidelity until a suitable representation was obtained.

3.1 Coulomb

One of the simplest friction models is the Coulomb model. This model embodies the basics of opposing motion but neglects the associated dynamics. An important characteristic of this model is that it will always dissipate the overall energy in a system. This is hard to simulate, as it can produce stiff differential equations. The other important characteristic is that the friction will oppose the relative surface velocity between two objects. Simulation implementation is discussed below.

The scalar version of the Coulomb model is defined by Equations 2 and 3, where μ is the friction

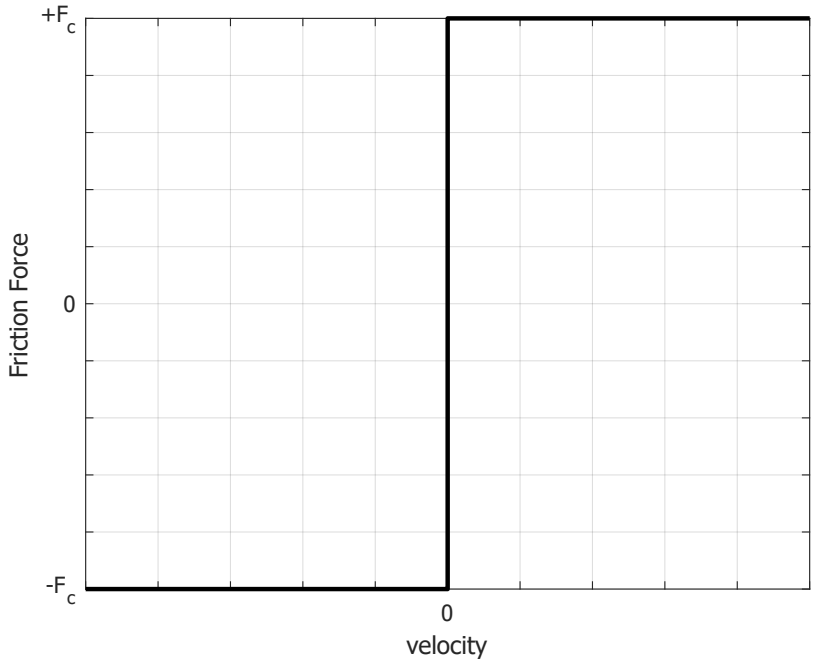

Figure 3. Coulomb operating regime

coefficient and N is the normal force applied to the surface. The Coulomb friction model has three simple operating regimes. The first regime is the trivial case at zero velocity and zero force input. In this case, there is no friction force as the friction has nothing to oppose and cannot add energy to the system. The second case is when there is an external force, F_{ext}, applied to the system, but it is not enough to break the frictional contact. In this regime, the friction force, F_c, has no velocity to oppose, but it does not exceed the external force. Thus, the friction force can only be as big as the external force in order to prevent the surfaces from moving. The last regime is when the body has enough force to overcome the friction force and thus the friction force is a constant on the body in the direction opposite the velocity. If there is no force on the system but the momentum of the body is enough to persist through the impulse of the friction encounter, then this regime is also valid.

$$F_c = -F_{ext} sign(v), \quad \mu N > F_{ext} \tag{2}$$

$$F_c = -\mu N sign(v), \quad F_c < F_{ext} \tag{3}$$

In simulation it is important to book keep two things that go hand in hand with the friction basics discussed above. The first is that the energy of the system should never be increased via friction. With finite integration time-steps, this can become a problem. An easy remedy is to track the momentum change due to the external forces with and without friction. If the momentum is larger after friction is applied, the friction force is adjusted to take the momentum to zero instead. This can be further complicated for a rotational body if the inertia is not isotropic. In this case, energy conservation can be forced via additional simulation logic so that the energy of the system will never be increased. Another condition that needs to be satisfied is the velocity reversal. The

velocity should never be reversed via the Coulomb friction formulation. With knowledge of the time step and the current friction state, the friction force can be adjusted to bring the body back to zero velocity. Naive implementation will result in chatter about zero as the Coulomb model forces the body back and forth over its zero velocity state.

3.2 Dahl

The Dahl model was developed by Philip Dahl in the 1960's to model ball bearing contact dynamics. This friction implementation was developed to mimic the behavior of the stress-strain curve in materials and approximate the surface deformation that occurs during friction [3, 4, 5]. To visualize this, Figure 4 shows a surface with asperity junctions modeled as "bristles" in contact with another surface. Asperity junctions are the local surface indentations that contact and transmit forces between each body. As the surface moves, the bristles deflect and exert a force on both surfaces. The sum of all the bristle forces on an object is the friction force between the two surfaces.

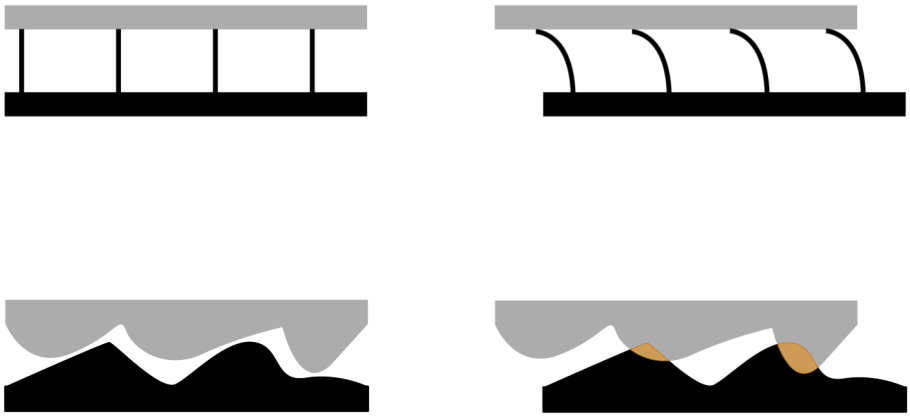

Figure 4. Dahl model bristle deflection

The equations for this model can be found below in Equations 4-5. In this two-dimensional form, they are the vector extensions of the original Dahl friction dynamics. The $\vec{z}$ state is the vectorized linear deflection of the bristle representing the bulk dynamics of all the asperity junction contacts between two surfaces. This allows the bristle to account for motion in multiple axes (i.e., pitch and yaw), thus taking into account the vector friction effect. The α term is used to scale the Dahl state equation. α values greater than one fit ductile materials while values less then one describe brittle materials. The F_c value is calculated in the same manner as the Coulomb equation except that it is always μN in the Dahl case. There is no need to handle the cases around zero because the bristle state equation makes those dynamics much less stiff than their Coulomb counterparts. The last value of interest is σ_0. This is the stiffness of the bristle and relates the bristle displacement to force and generally defines how fast the system will reach its maximum friction state. The $\frac{d\vec{z}}{dt}$ formulation is what leads to the output shape that models the stress-strain curve. One note about this model is that it is position-dependent, but not velocity-dependent. Thus, the friction force will not be affected by larger velocities along the same path of travel. In Figure 5, one can see the effects of a range of sawtooth profiles that vary by velocity. The friction force only depends upon the position in this model and does not change as the sawtooth profile is commanded at a faster or slower rate.

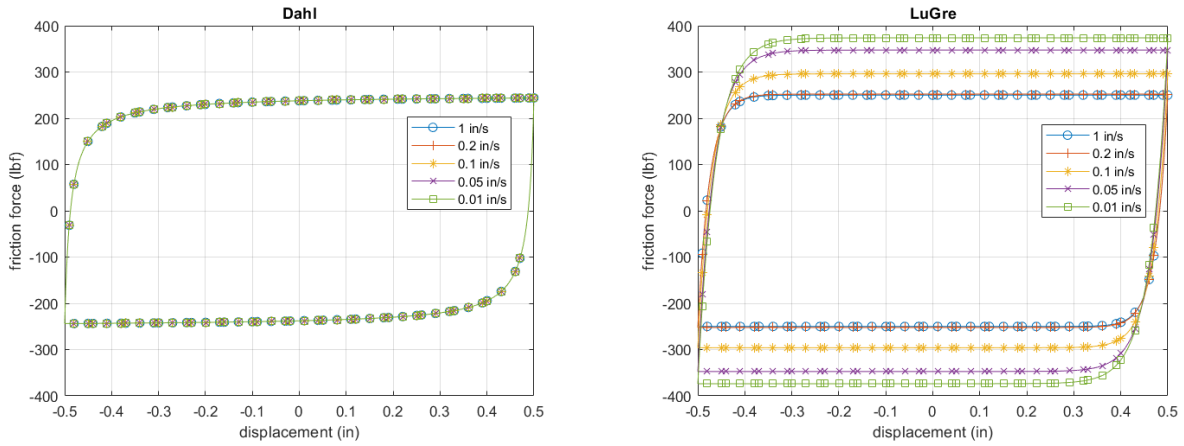

Figure 5. Dahl (left) and LuGre (right) position and velocity dependence

$$\frac{d\vec{z}}{dt} = \left(\vec{v} - ||\vec{v}|| \frac{\sigma_0 \vec{z}}{F_c}\right)^{\alpha} \tag{4}$$

$$\vec{F}_f = \sigma_0 \vec{z} \tag{5}$$

3.3 LuGre

The LuGre model is an extension of the Dahl model researched by the Laboraoire d'Automatique de Grenoble research group in 1993 [6]. This model sought to extend the Dahl model to include the Stribeck effect, friction damping, and a viscous term. The Stribeck effect captures the common phenomenon whereby the static frictional forces are greater than the forces during dynamic motion. As the object starts to move, the friction will resist the stiffness of the asperity junction contacts between two surfaces as they move against one another in a regime often called stiction. During the initial movement, the deflection of asperities is slow and simultaneous, creating a larger friction force compared to when the object is in motion over the asperities. As velocity between the two surfaces increases, the asperities do not stick together and instead are sliding over each other. This leads to two different observed regimes of the friction force. This effect demonstrates the stick (static) versus sliding (dynamic) regime of the LuGre model. Once the asperity junctions reach their maximum deflection, they will break and result in sliding motion. Until that point, the surfaces are locked together and move elastically. Thus, the Stribeck effect models how the surfaces move as the body transitions from sticking to sliding. The other phenomena modeled by the LuGre model are the damping and viscous terms. The friction damping applies a simple linear damping term to the rate of the pseudo-deflection and the relative motion between the two surfaces.

The model operates along the same assumptions as the Dahl model by modeling the friction force as a sum of the "bristle" deflection. The additional parameters are γ, v_s, σ_1 and σ_2. The quantity γ is the ratio of the static friction (stiction) coefficient to the dynamic friction (sliding) coefficient, while v_s parameterizes the velocity regime between the static and dynamic friction coefficient as seen in Equation 6. As the velocity magnitude increases, the friction coefficient approaches the dynamic coefficient of friction, which is smaller than the static coefficient. Equation 6 is then used to determine the Stribeck friction (F_s) used in the $\vec{z}$ state derivative calculation. Equation 7 looks

very similar to that of the Dahl formulation. The one difference is that here the F_s value is not a constant. The only other difference between the models is the inclusion of the σ_1 and σ_2 terms in the force calculation. This includes the damping effects of the bristle displacement derivative and the viscous effects of the velocity, respectively. The effects of these additional parameters are captured in Figure 5. All parameters are the same as the Dahl model besides the additional components of the LuGre model. The range of different velocity conditions produce different responses in the LuGre Model case. In this example, the parameter v_s is 0.1 $\frac{in}{s}$. At the lower velocity values, the friction force is greater as it is in the stiction regime of the LuGre model. As the velocity approaches v_s, the stiction effect starts to become less influential. When the velocity is a magnitude of 10 times v_s, the model behaves much like the Dahl model, as it is out of the stiction regime.

$$F_s = F_c \left(1 + (\gamma - 1)\, e^{-\left(\frac{||\vec{v}||}{v_s}\right)^2}\right) \tag{6}$$

$$\frac{d\vec{z}}{dt} = \left(\vec{v} - ||\vec{v}|| \frac{\sigma_0 \vec{z}}{F_s}\right)^{\alpha} \tag{7}$$

$$\vec{F}_f = \sigma_0 \vec{z} + \sigma_1 \frac{d\vec{z}}{dt} + \sigma_2 \vec{v} \tag{8}$$

LuGre model has several advantages: it still has relatively few parameters, and it is easy to implement in simulation due to the behavior about the zero velocity condition. All parameters also model physical friction phenomena, so they are not necessarily just fitting a curve to a distribution of test data. Issues with the LuGre model include over-fitting for very simple friction behavior and an inability to capture friction force reductions at lower velocities for systems that are not well characterized by viscous friction.

4 ADDITIONAL TVC MODELING FIDELITY

The keys to describing the behavior seen in test involved taking account of some of the other dynamics that affect the engine movement. There is a host of well-known phenomena including gyroscopic effects of the turbopumps, gimbal bearing material wear, and the loads imparted on the engine by its thermal blankets. These effects were not shown to explain the observed response. The remaining sensitivities to the load stiffness and core stage modes were examined with higher order models including Extended Simplex (Simplex model with additional DoF for the structure) and the Multiple Actuator Stage Vectoring simulation (MASV) modal model. These models are described in greater detail in the companion papers.[14, 17]

To support the present analysis, an improved model was developed, called Two Actuator Operational Simulation (TAOS), which extends the traditional 1- DoF model and incorporates a fully-coupled 6-DoF model of the engine to account for cross-axis coupling, translation due to thrust loads and actuator forces, and 3D friction applied to the spherical gimbal bearing surface. The TAOS dynamics engine is a simplified elastic multibody formulation derived from Lagrange's equations in quasi-coordinates using a coordinate frame whose origin is fixed in space. The elastic bodies are constrained to the rigid-body engine using Witkin's method, and the rotational kinematics are expanded to second order, providing geometric displacements that are accurate over the entire operating range of engine deflections. A detailed description of the TAOS dynamics is beyond the scope of the present discussion, but will be described in a forthcoming paper.

Using the TAOS model, some of the observed effects in GRHF were isolated to depend the structure of the gimbal itself. Due to higher than expected structural compliance, the actuator and thrust loading on the gimbal was enough to induce measurable displacement of the gimbal structure. This motion suggests beam-like dynamics in the engine gimbal halves (albeit at very high frequencies) and produces artifacts in the frequency and time domain. It also affects the friction environment, as the gimbal halves move relative to each other.

Finally, friction was found to be attenuated when considering the vibration environment experienced by the engine at low angular velocities. Despite the clear presence of friction in the MPTA hot fire responses, after Shuttle exhibited no evidence of limit cycling in flight, general conclusions were drawn that the vibration environment produced by the engine and vehicle made the friction in the gimbal bearing negligible at low gimbal rates. Since these initial conclusions, there have been more studies of the surface-to-surface interactions and mechanics and materials that affect the friction and vibration interactions [7, 8, 10, 11, 12, 9]. The authors applied the findings of these newer studies to show how the engine friction environment may have been influenced by external vibration.

4.1 Modeling in Multiple Dimensions

The first of the important characteristics is the coupled nature of the TVC system. The initial modeling approach approximated the TVC response using a single DoF. This was convenient for linear analysis and simulation, and appeared to describe the system well, but further analysis suggested that a two-axis model would be required. TAOS was initially created to investigate this discrepancy. Two actuators were attached to a single engine to inspect whether the cross axis effects could be demonstrated with a 3-DoF rotation within the gimbal. Subsequently, in order to model radial displacements of the center of mass and the thrust vector, translation degrees of freedom were incorporated. The engine and gimbal system will translate in space under thrust and TVC loads, as the stiffness of the thrust structure and gimbal are finite. This translation, in turn, affects the kinematic relationship of the actuator attach points.

With a gimbal bearing model in 3 DoF, friction torques are coupled so that the bulk motion produces friction, including the effects of roll motion.Since in the RS-25 gimbal bearing the load is accepted by a single bearing surface, motion in one axis can cause sliding in the opposing axis. That is, motion in the other axis can effectively act as a dither, causing a reduction in the apparent friction in the commanded axis. This effect was present in the GRHF test; due to limited test time,command profiles included high frequency inputs in one axis while the other axis had low frequency input, as seen in Figure 6 for the GRHF yaw channel piston telemetry. When comparing the yaw command to the yaw engine output, the apparent reduction in gain is higher when the pitch axis is not commanded (first peak) versus when the it is commanded (second peak). Likewise, the apparent phase lag begins to increase when the pitch axis is not dithering the yaw channel.

4.2 Compliance of the Gimbal Structure

Compliance of the gimbal structure can be defined as the resultant deflection due to a force or torque input, or the inverse of the stiffness of the gimbal structure. In previous modeling, the compliance of the gimbal structure had been considered to be sufficiently stiff and this, along with the zero friction assumption, led to the use of a lumped load stiffness parameter as sufficient to capture the structural stiffness relevant to TVC. In the process of eliminating possible causes of the difference in the ambient versus hot fire test, the structure of the gimbal was analyzed in detail.[17] The

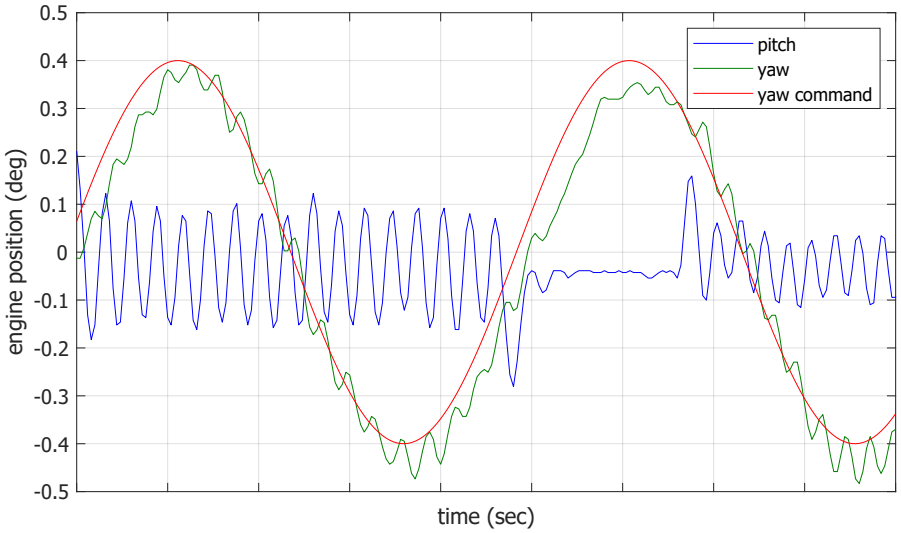

Figure 6. GRHF piston telemetry data showing axis crossover from pitch to yaw channel

structural team found that the load path along the gimbal was different in ambient versus GRHF. This is because when the vehicle is thrusting, the gimbal joint (as seen in Figure 7) is compressed and both halves of the gimbal are in contact along the spherical surface of the joint. In the non-thrusting condition, the gimbal is not compressed, and the load is transferred through the "ears" of the gimbal. In Figure 7, one can observe how the two pieces of the gimbal are assembled and held together by the shaft between them. When approximating the behavior of the gimbal joint as a stiffness matrix for flight control, it is important to separate the two conditions. Thus, when considering the thrusting and non-thrusting conditions, different stiffness approximations are required. This new effect is now included in the model of the engine in TAOS by expanding the system to model the gimbal as a cantilever beam attached to a free-free beam, attached to the RS-25 engine. This includes the stiffness matrices for the seat (cantilever component) and body of the gimbal (free-free component).

Modeling the gimbal compliance is an important part of modeling the TVC subsystem performance. It is usually assumed that the gimbal is sufficiently stiff to neglect, but in the presence of very high thrust loads, the additional DoF play a role in the dynamics of the thrust vector. For example, the gimbal will compress when the thrust is applied, and the whole system will move up in the axial direction. Although the compliance is small, it affects the load path that the actuator experiences along its direction of its motion. Another example is when the actuator force is applied. In the simple models, the actuator extension or retraction becomes a torque that directly is applied to the engine gimbal joint. In the higher order models, the torque and force are transferred first to the bottom half of the gimbal and then the response is transferred to the top half of the gimbal. The gimbal will comply in the direction it is being pushed by the actuator. This is in addition to the actual gimbal rotating at the gimbal joint interface.

Some effects on the frequency response are seen in Figure 8. Both of these results are produced with TAOS, but in one, the model has all structural and nonlinear components removed, so that

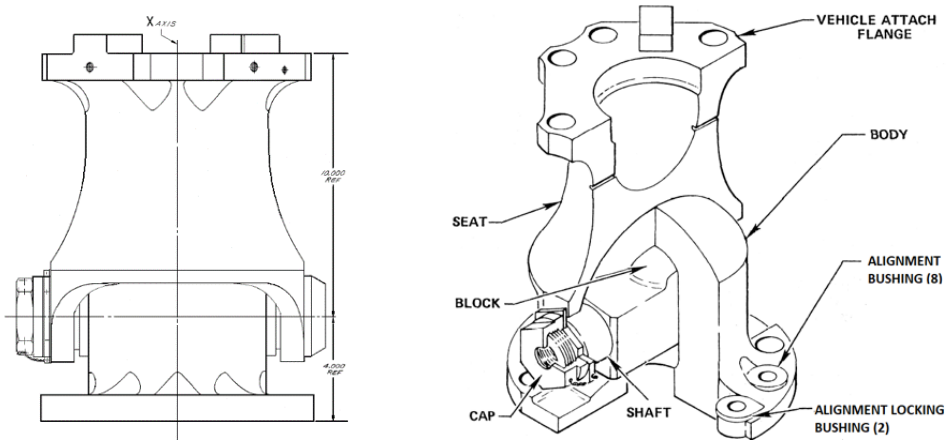

Figure 7. RS-25 Gimbal bearing assembly

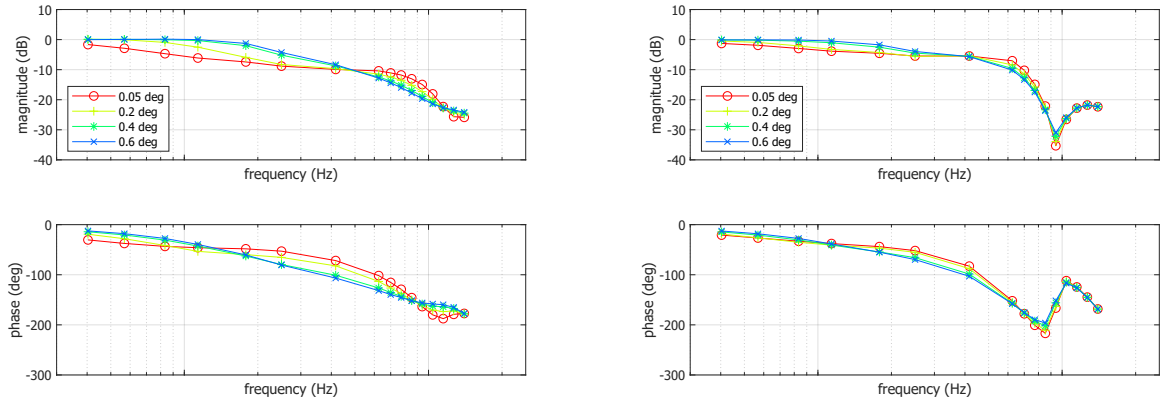

Figure 8. Comparison of Simplex (left) and TAOS (right) piston response with the best fit parameter set

it behaves like its linearized counterpart. Multiple amplitudes are included to show the amplitude dependence of each model as well. The responses are vastly different due to the structural dynamics included in the second model. The notch characteristic due to load resonance disappears with the friction level in the case of the simplified model, but not in the higher fidelity model. In addition to this, the amplitude dependence is much more drastic in the case of the simplified model. Both of these effects show that the inclusion of the gimbal structural dynamics change the core behavior of the system with friction and are required to fully verify the system performance. These effects are discussed more fully in a companion paper.[17]

4.3 Vibration Effects on the Gimbal Bearing

It was observed that in order to correlate with test, the mechanics of the two movable surfaces of the RS-25 gimbal bearing in 3D space must be considered. These surfaces produce friction when there is relative motion between the two surfaces and a normal force between them. This friction is a function of the contact geometry, material, normal force magnitude, and the magnitude of relative

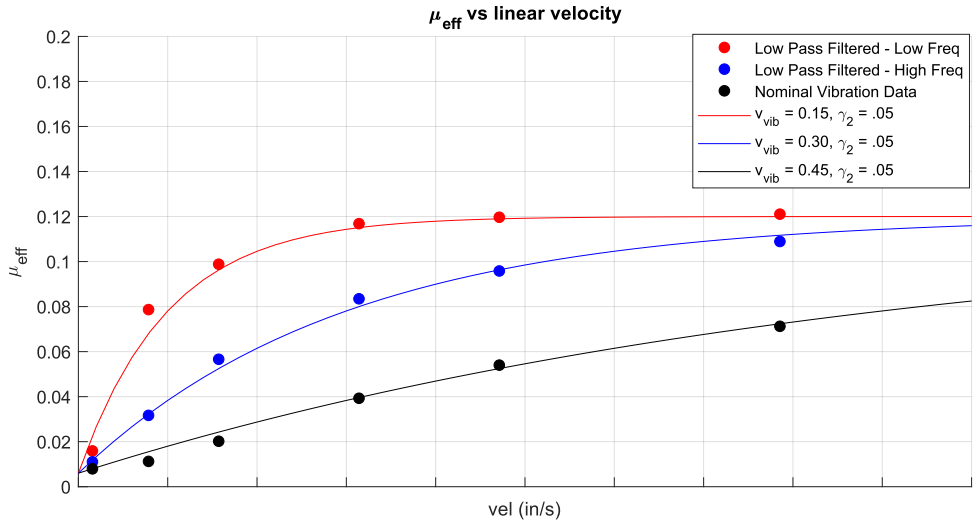

Figure 9. Vibrations effects on LuGre Model at different filtering conditions

motion between the two surfaces.

When vibration occurs, the motion between the surfaces is affected by an additional component. The vibratory motion can be in one of three directions, normal to surface contact, in the direction of motion, and in-plane but transverse [10]. The biggest factor in all cases of vibratory motion is that the surfaces never stop moving relative to each other and are constantly brought out of the stiction regime. When in the normal direction, the vibratory motion will tend to separate the asperities from each other. This will reset and/or prevent large deflections of each asperity when the relative velocity is low. The motion in plane tends to cause decreases in friction force, as the asperities get moved away from their contact, thus never allowing the full deflection of most of the asperity junctions. The transverse oscillations can also decrease the friction force. This is due to movement of the friction force vector out of the direction of the bulk body motion. If there is constant motion in one direction with vibration, the friction force will oppose the local relative velocity. With vibration, this will not be in the same direction as the constant motion of the surface and will result in an apparent decrease in the friction force opposing the motion of the two surfaces, as the friction force vector is affected by the additional vibratory motion. In a rocket gimbal, it is expected that the dominant vibration will be in-plane as the oscillation is unlikely to overcome the thrust load. The vibration environment of a rocket gimbal bearing leads to a spectrum of oscillation frequencies in pseudo-random direction instead of an oscillation at a discrete frequency in a single direction as most of the literature employs [7, 8, 9, 10, 11, 12]. The friction is then affected at low velocities because the local direction of motion is changing rapidly when the vibration velocity is greater than or equal to the bulk velocity. This reduces the ability for friction to manifest in a given direction until it overcomes the local velocity changes due to vibration.

The LuGre model has been the most accurate when trying to replicate the observed behavior of the RS-25 gimbal bearing. The effects the LuGre model capture such as surface stiffness, frictional memory and damping, can be adjusted to closely replicate what was observed in the GRHF engine

response. However, an issue was still present in the low-velocity regime as there was little to no stiction in the test data, even under thrust load. This effect was not supported by the LuGre model, because the stiction force was always expected to be higher than the steady state friction force. The model was adjusted to include a term for vibration effects at low velocities. This effect is captured in the Coulomb force calculation shown in Equation 9.

$$F_c = \mu N \left(1 - (\gamma_2 - 1)\, e^{-\left(\frac{||\vec{v}||}{v_v}\right)}\right) \tag{9}$$

The structure of this change is almost identical to the Stribeck curve. However, Equation 9 is formulated so that friction can be decreased at low velocity, rather than increased. This is accomplished through the definition of ratio of minimum friction over steady state friction (γ_2) and the vibration velocity term (v_v). With this effect, the friction force will exponentially approach the steady state Coulomb force as a function of the ratio of the velocity of the body to the velocity of the vibration. The vibration velocity is an empirical value that does not map to a direct physical motion. Instead, it is the bulk vibration effect on the body that encompasses the total power spectrum of the vibration, adjusted to best represent the observed vibration power spectrum.

Vibration data for the RS-25 engine in the firing condition was derived from static firing data obtained on the A-1 test stand. When estimates of the vibration spectra were added to force the gimbal bearing in the TAOS model, the friction was significantly attenuated for small velocity motions. In terms of the bristle, the induced transverse motion prevents the bristle from reaching maximum deflection and transmitting the maximum friction force. This full effect is captured because TAOS captures all directions of motion of the gimbal at once instead of the assuming planar motion in either pitch or yaw. The surface geometry and interactions are not modeled, but the effects on the engine due to the forcing input are. At small velocities the vibration will induce random motion that makes up a large amount of the motion in the gimbal bearing. As velocity is increased, this motion becomes smaller and smaller compared to the bulk velocity of the actuator movement and the friction approaches its nominal value. Figure 9 shows a comparison between the standard LuGre model with various simulated vibration environments against the results with the modified LuGre equation. The scattered points are the standard LuGre model average over a constant velocity command to the actuator and the solid lines are the friction coefficient calculated from the modified LuGre model equation. As shown, the model equation matches with the effect of adding the simulated vibration directly into the model. This agrees well with the previous literature [8, 11]that suggests that higher frequency oscillations attenuate friction well across many types of systems.

5 SIMULATION VS TEST DATA

In the following subsections, a comparison between the TAOS high-fidelity model and the GRHF data is summarized. After extensive model fitting to parameterize the friction models and incorporate the gimbal compliance, the TAOS model is able to faithfully reproduce the responses observed in GRHF. Results from TAOS were combined with other tools to support the flight rationale for Artemis I.[18]

5.1 Frequency Response

In TAOS, the frequency response of the system is extracted at discrete frequencies via the describing function reconstruction analysis techniques detailed in reference [16], so as to exactly duplicate

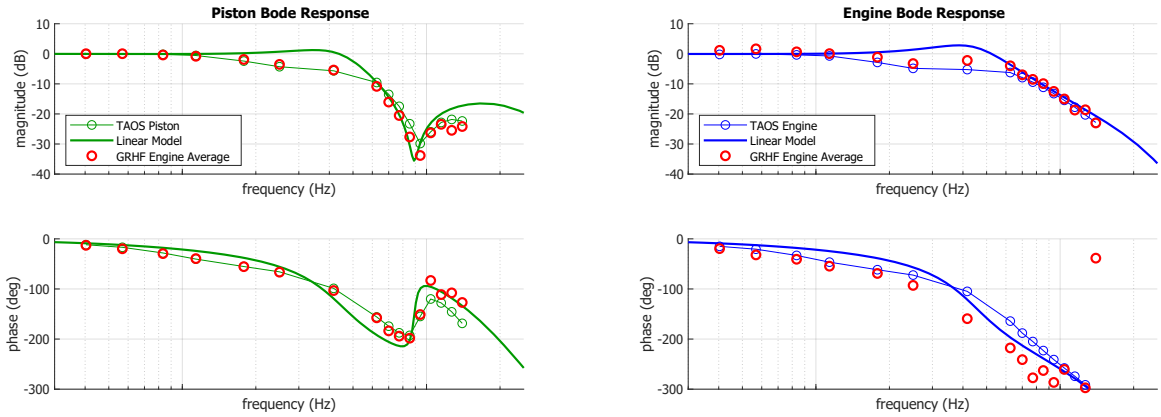

Figure 10. Yaw piston (left) and engine (right) responses

the test profiles that were applied to the flight hardware. The analysis in TAOS attempted to reproduce two different measurements extracted from the Green Run test series. The first is the piston measurement that represents the displacement of the actuator piston. The second is the engine position, which is determined via string potentiometer length measurements between the engine and the thrust structure.[16] Figure 10a depicts the simulated actuator piston response compared to that of the piston response observed during GRHF. The red circles are the response that was observed in the GRHF data set, while the TAOS simulated response can be seen as the green circle marks. The thick solid green line is the heritage linear simplex model. Figure 10b shows engine response with the GRHF as red circles, TAOS simulation as blue circles, and the heritage simplex model as the thick solid blue line.

As can be seen, TAOS piston response (green circles) and GRHF piston test data (red circles) agree for the entire frequency range. At lower frequencies, TAOS predicts the gain to approach DC at low frequency, which is similar to test. The mid frequency region is where friction begins to degrade the ability of the actuator to fully satisfy the command. The linear model, while adjusted to match the load stiffness observed in the piston notch responses, does not have friction, structural or vibration effects. It is important to note that the frequency range where the nonlinear and linear models differ can shift if the engine is not moving both axes simultaneously; i.e., the effects of moving one axis at a high frequency and one at a low frequency has an attenuation effect on the gimbal friction. If each TVC axis was interrogated separately, an additional decrease in gain due to friction would be expected.

Both the model and the test data depict the load resonance near 9.5 Hz, using a corrected value of the load stiffness corroborated by the finite element model.[14, 17] The average of the GRHF test data has a slightly deeper notch, e.g., lower apparent load damping. This is attributed to measurement error and damping assumptions that were not investigated in this study. At higher frequencies, the differences in the model and test data can be related to structural modes of the vehicle on the test stand and is discussed further in the companion paper.[17]

Figure 10b shows the simulated engine response versus the engine response estimated from GRHF test data, which also exhibits good agreement across the response spectrum. Although

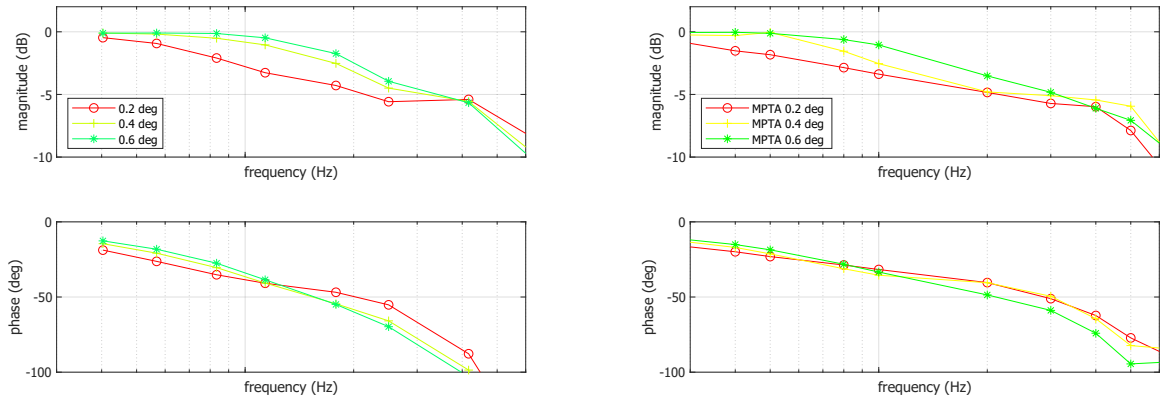

Figure 11. Amplitude dependence of TAOS (left) and Space Shuttle MPTA (right)

the quality of this data is lower than that of the piston measurements due to geometric calibration errors,[16] the same reduction in gain due to friction appears in the low frequency range.

It is important to note that while the GRHF test profile was restricted to two command amplitudes, amplitude dependence is a major factor in the development of friction-induced limit cycles in the closed-loop flight control response. Historical Space Shuttle Main Propulsion Test Article (MPTA) data was used to support further analysis, since these data include multiple amplitudes, albeit with frequency resolution too low to determine effects on the load resonance. These results are shown and compared in Figure 11, where TAOS piston response data for SLS over a range of amplitudes is compared with STS MPTA data. Both data sets exhibit similar trends. The lower amplitude commands have a larger friction to actuator torque ratio, thus they suffer a larger amount of gain reduction and phase distortion. It is noted that the important amplitude-dependent phase response can not be captured using a Coulomb model.

5.2 Step Response

Most of the time series response analysis was centered around the step response data, where three sets of step commands were issued having amplitudes of 0.2, 0.4, and 0.6 degrees. Due to nonlinearities, the "deflect" dynamics (null piston position to the commanded amplitude) differs from the "return" dynamics (commanded amplitude back to the null position).* This data can be seen in Figure 12a and 12b as the deflect (left) and return (right) response for the engine. The signal that is compared to the TAOS model is the string potentiometer based engine position measurement from GRHF. As discussed in the companion paper,[16] true offset during the steps could not be deduced from string pots. Thus, it was assumed all steps reached their commanded value and started from null. For comparison, TAOS data is plotted with the same assumption. The shape of each of the signals appears to agree well with what was seen in the GRHF test data. The shapes are all heavily damped and show a reduction in transient response performance due to friction. Notably, the return time series shows a larger time constant for the decay than is seen in test data, but TAOS reproduces the character of the oscillations.

*Depending on the engine DoF, this may involve either an extension or retraction of the associated actuator.

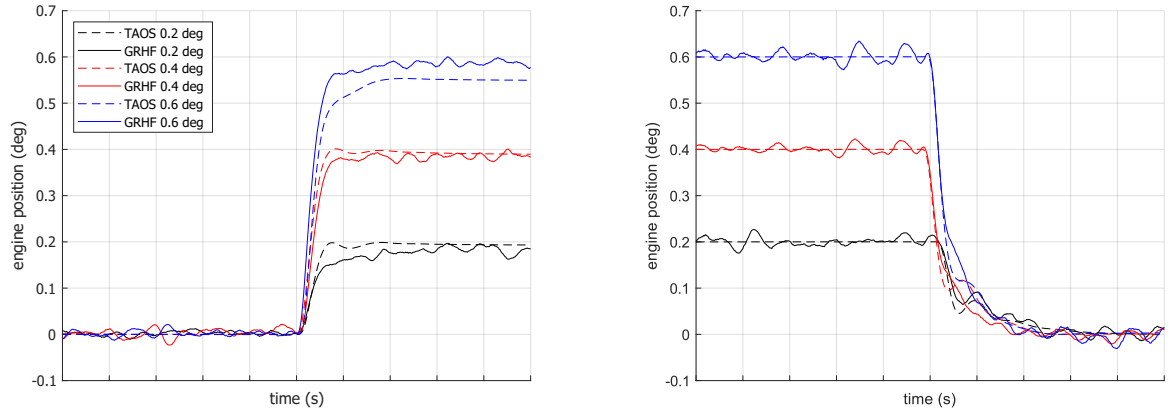

Figure 12. Engine time series response to step command

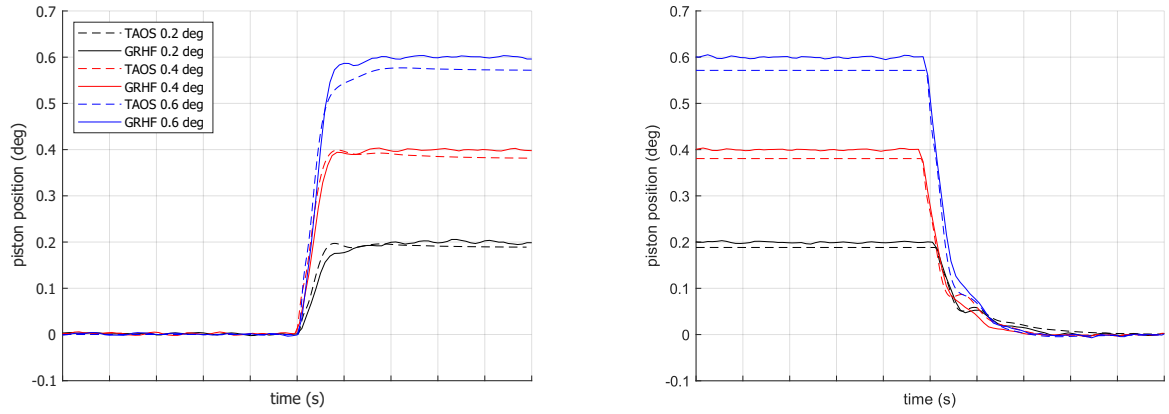

Figure 13. Piston time series response to step command

In Figures 13a and 13b, the piston response data from GRHF is compared to its model equivalent in TAOS. In this case, the data from GRHF is trusted becasue of experince in heritage applications. Due to confidence in the measurement, the comparison of piston data was the main driver for friction fits to the GRHF profile.The offset present in the TAOS piston data is due to a steady state friction force. This is a lingering limitation of modified LuGre approach. The modeled response during the return to zero command portion matches the shape of the test data well and captures both the time constant and slope changes apparent in test. Also noted during Shuttle MPTA [23], the difference in deflect and return can be attributed to the relationship between the friction loaded gimbal and the deflection of distributed stiffness in both the gimbal and actuator load paths.

6 CONCLUSIONS

The GRHF test series supported complete end-to-end verification of the SLS Core Stage thrust vector control and propulsion systems. It was especially important for the flight controls team as it yielded critical information leading to advances in understanding of the TVC behaviors anticipated for flight. After analysis, the team concluded that the system had much more friction than was

initially assumed. This had a large effect on the response characteristics of the TVC system and led to development, verification, and validation of higher order models that were able to describe the system more accurately. This brought about the development of TAOS, Extended Simplex, and MASV into the analysis space.

The most impactful modeling additions on the TVC response included the vector friction effect, structural compliance of the gimbal, and the vibration environment of the engines. Since the RS-25 gimbal is a spherical bearing, in Green Run the simultaneously-commanded test responses could not be represented with individual axes. A detailed model of the gimbal structural compliance was required to accurately model the transfer of friction loading between the engine and stage structure. This also included the effects of the thrust and actuator- induced deflections that changed the dynamics of the gimbal and the kinematics of the actuator attachments. This shows up in the frequency domain by affecting the total stiffness of the engine system, and thus the location of the apparent load resonance. These effects were also found to to be a key in small-amplitude step responses, affecting the return-to-zero offset and and its characteristic "hesitation" behavior. Finally, the vibration environment near the gimbal was found to affect the friction in the gimbal joint. This environment is likely produced by high-frequency engine thrust dynamics, high-frequency structural dynamics, and vibroacoustic noise.A modified form of the LuGre model showed an excellent match to the friction-attenuating effects of the vibration environment.

The SLS Artemis I launch vehicle flew its first and highly successful ascent trajectory on November 16, 2022 with the flight control system performance tracking very close to nominal pre-flight predictions.[18] The contributions of the modeling efforts described herein and in the companion papers were critical in developing the flight control design and flight rationale that led to this overwhelming success for the next generation of human-rated launch vehicles.

ACKNOWLEDGMENTS

The authors are grateful to John Wall for his GN&C expertise throughout the analysis process as well as support in development of the models used in this study. The authors would like to acknowledge the efforts of Ivan Bertaska (NASA MSFC) and the entire SLS Ascent Controls Working Group for their support and review of these analysis techniques. This work was supported by the NASA Marshall Space Flight Center under contract number 80MSFC18C0011.

REFERENCES

[1] Olsson, H., Åström K.J., Canudas de Wit, C., Gäfvert, M., and Lischinksky, P., "Friction Models and Friction Compensation," *European Journal of Control*, vol. 4, no. 3, pp. 176-195, 1997.

[2] Armstrong-Hélouvry, B., Dupont, P., and Canudas de Wit, C, "A Survey of Models, Analysis Tools and Compensation Methods for the Control of Machines with Friction," *Automatica*, vol. no. 7, pp. 1083-1138, 1994.

[3] Dahl, P. R., "A Solid Friction Model," Space and Missile Systems Organization, TR-77-131, 1977.

[4] Dahl, P. R., "Measurement of Solid Friction Parameters of Ball Bearings," Space and Missile Systems Organization, TR-77-132, 1977.

[5] Dahl, P. R., "Solid Friction Damping of Mechanical Vibrations," *AIAA Journal*, vol. 14, no. 12, pp. 1675-1682, 1976.

[6] C. C. de Wit, H. Olsson, K. J. Astrom and P. Lischinsky, "Dynamic Friction Models and Control Design," in *1993 American Control Conference*, pp. 1920-1926, 1993.

[7] Hess, D. P., Soom, A., and Kim, C. H., "Normal Vibrations and Friction at a Hertzian Contact under Random Excitation: Theory and Experiments," *Journal of Sound and Vibration*, vol. 153, no. 3, pp. 491-508, 1991.

[8] Leus, M., and Gutowski, P., "Analysis of Longitudinal Tangential Contact Vibration Effects on Friction Force Using Coulomb and Dahl Models," *Journal of Theoretical and Applied Mechanics*, vol. 46, no. 1, pp. 171-184z, 2008.

[9] Mao, X., Popov, V. L., Starcevic, J., and Popov, M., "Reduction of Friction by Normal Oscillations. II. In-Plane System Dynamics," *Friction*, vol. 5, no. 2, pp. 194-206, 2017.

[10] Popov, M. and Qiang, L., "Multi-mode Active Control of Friction, Dynamic Ratchets and Actuators," *Phys Mesomech*, vol. 20, no.5, pp. 26-32, 2017.

[11] Wang, P., Ni, H., Wang, R., Liu, W., and Lu, S., "Research on the Mechanism of In-Plane Vibration on Friction Reduction," *Materials*, vol. 10, no. 9, 2017.

[12] Pohrt, R., "Friction Influenced by Vibrations: A Refined Contact-Mechanics View on Lateral and Rotational Oscillations," *Frontiers in Mechanical Engineering*, vol. 6, 2020.

[13] Stuart, B., et al., "Overview of the SLS Core Stage Thrust Vector Control System Design," AAS 23-152, American Astronautical Society Guidance, Navigation, and Control Conference, February 2023.

[14] Orr, et al., "Advanced Modeling of Control-Structure Interaction in Thrust Vector Control Systems," AAS 23-153, American Astronautical Society Guidance, Navigation, and Control Conference, February 2023.

[15] Stuart, B., et al., "Core Stage TVC Systems Engineering Challenges in Reusing Heritage Hardware," AAS 23-154, American Astronautical Society Guidance, Navigation, and Control Conference, February 2023.

[16] Wall, J., et al., "Design, Instrumentation, and Data Analysis for the SLS Core Stage Green Run Test Series," AAS 23-156, American Astronautical Society Guidance, Navigation, and Control Conference, February 2023.

[17] Moore, R., et al., "Structural Dynamics Observations in Space Launch System Green Run Hot Fire Testing," AAS 23-157, American Astronautical Society Guidance, Navigation, and Control Conference, February 2023.

[18] Wall, J., et al., "Flight Performance and Stability of Space Launch System Core Stage Thrust Vector Control," AAS 23-158, American Astronautical Society Guidance, Navigation, and Control Conference, February 2023.

[19] Thompson Z., "A Mathematical Model for a Space Vehicle Thrust Vector Control System," MS Thesis, University of Tennessee, NASA Report 67-34613, Aug 24, 1967.

[20] McDermott, et al., "Space Shuttle Ascent Flight Control Actuation Subsystem Data Book," SSD93D0595, Rockwell, September, 1993.

[21] Altenbach, R., McDermott, W., and Lam, L., "Characterization of Gimbal Bearing Friction In the SSME-TVC Actuation System," Boeing Informal Technical Discussion, May 2005.

[22] McDermott, W., "TVC Actuator System Overview," Ascent GN&C/Actuators Technical Exchange Meeting, March 2004.

[23] Gerstner, B. A., "MPT Engineering Analysis Second Interim Report Static Firings S/F-5A Through S/F-12" Rockwell Report STS 81-0254, May 1981.